Electron–interface-phonon interaction and scattering in asymmetric semiconductor quantum-well structures

Jun-jie Shi
*China Center of Advanced Science and Technology (World Laboratory), P.O. Box 8730, Beijing 100080, China and Department of Physics, Henan Normal University, Xinxiang 453002, Henan, China**

Shao-hua Pan
*China Center of Advanced Science and Technology (World Laboratory), P.O. Box 8730, Beijing 100080, China and Institute of Physics, Academia Sinica, P.O. Box 603, Beijing 100080, China**
(Received 22 August 1994; revised manuscript received 9 December 1994)

The interaction Fröhlich-like Hamiltonian between an electron and interface optical phonons in asymmetric single and step quantum-well (QW) structures is obtained and studied. We observe that the behaviors of electron–interface-phonon coupling functions as functions of wave number k have two anomalies. The first is that, in an asymmetric single QW and general step QW, the interaction between an electron and the lowest frequency interface mode is large in the vicinity of the Brillouin-zone center. The second anomaly is that in step QW's the interaction between an electron and the fifth interface mode has a maximum which relates to the inflection point in the dispersion (ω_5-k) plot. The physical origins of these two anomalies have been analyzed. The electron–interface-phonon-scattering rates for intrasubband and intersubband transitions in asymmetric single and step QW structures are also calculated and are given as functions of well width, step width, and step height. It is shown that the electron scattering depends strongly on the potential parameters, and the usual selection rules for these transitions break down in asymmetric heterostructures.

I. INTRODUCTION

It is well known that electron–interface-phonon interaction and scattering are important in semiconductor heterostructures such as quantum wires, quantum wells (QW's), and superlattices. Electron–optical-phonon scattering controls such phenomena as the cooling of optically excited carriers on the picosecond time scale as well as transport and optical properties at room temperature; thus reliable values for the scattering rates in realistic structures are needed for quantitative studies of their properties.

Recently, Lin, Chen, and George investigated the optical-phonon modes,[1] electron-phonon interaction,[2,3] polaron states,[3] and magnetopolaronic effect[2] in QW's. Their results have quantitatively demonstrated the importance of the electron–interface-phonon interaction in a QW structure. The electron–interface-phonon interaction has been investigated in symmetric[4–6] and asymmetric single QW's.[7] We have studied the interface (and surface[8]) optical-phonon modes in four-layer[9] (and finite double[8]) heterostructures of polar crystals. The electron–interface-phonon scattering has also been studied for symmetric single QW's,[10,11] symmetric multiheterointerface structures,[12] and graded QW's of $Al_xGa_{1-x}As$.[13] However, to date there has been little theoretical work on electron–interface-phonon scattering in asymmetric heterostructures such as asymmetric single and step QW structures which are of great practical importance. Jain and Sarma[14] pointed out that the electron–interface-phonon interaction and electron relaxation depend strongly on the potential parameters and boundary conditions in heterostructures. Therefore the study of the electron–interface-phonon interaction and scattering in these practically important asymmetric heterostructures is necessary for the further investigation of their properties. The purpose of this paper is to investigate the interaction Fröhlich-like Hamiltonian between an electron and interface optical-phonon modes and the electron–interface-phonon scattering in asymmetric single and step QW structures by using the orthonormal eigenmodes of interface optical-phonon modes given recently in Ref. 9, denoted as paper I hereafter. The present study may have significant consequences for device applications based on asymmetric layered structures where the electron–interface-phonon interaction is an important carrier relaxation mechanism.

This paper is organized as follows. In Sec. II, we outline the theory of the electron–interface-phonon interaction and scattering. In Sec. III, we present and discuss numerical results. Section IV gives a summary.

II. THEORY

A. Electron–interface-phonon interaction Hamiltonian

For the description of the electron–optical-phonon interaction Hamiltonian we follow strictly the work of Mori and Ando[5] and Wendler.[15] That is to say the electron-phonon Fröhlich-like Hamiltonian $H_{e-\mathrm{ph}}$ is obtained by quantizing the interaction energy $-e\Phi(\mathbf{r})$ of an electron at the position $\mathbf{r}$ with the electrostatic potential

produced by the phonons. For the interface optical-phonon modes given in paper I, the electron–interface-phonon interaction Hamiltonian can be obtained as

$$H_{e-\mathrm{ph}}=\sum_m\sum_k e^{i\mathbf{k}\cdot\rho}\Gamma_m(k,z)[\hat{a}_m(\mathbf{k})+\hat{a}_m^+(-\mathbf{k})]\ , \tag{1}$$

where the electron-phonon coupling function $\Gamma_m(k,z)$ (which describes the coupling strength of a single electron at position z with the mth optical phonon mode) is given as follows:

$$\Gamma_m(k,z)=\left[\frac{\hbar e^2}{8A\varepsilon_0\omega_m(k)}\right]^{1/2}\times\int_{-\infty}^{+\infty}dz' e^{-k|z-z'|}[i,\mathrm{sgn}(z-z')]\pi_m^*(k,z')\ , \tag{2}$$

where A is the cross-sectional area of the heterostructure, ε_0 is the absolute dielectric constant, the index $m(=1,2,3,4,5,6)$ labels the six branches of interface optical-phonon modes for a four-layer heterostructure and $m(=1,2,3,4)$ for an asymmetric trilayer heterostructure, $\omega_m(k)$ is the normal frequency of vibration obtained by solving the dispersion relation Eqs. (12) or (31) in paper I, and the step function is defined as $\mathrm{sgn}(z-z')=+1$ for $z>z'$ and $\mathrm{sgn}(z-z')=-1$ for $z<z'$. Substituting the eigenvector $\pi(k,z)$ expression [Eq. (18)] in paper I into Eq. (2), we find the coupling function $\Gamma_m(k,z)$ for a four-layer heterostructure as follows:

$$\Gamma_m(k,z)=\left[\frac{\hbar e^2}{8A\varepsilon_0\omega_m(k)}\right]^{1/2}\frac{1}{\sqrt{k}}f_m(k,z)\ , \tag{3a}$$

where $f_m(k,z)$ is defined as follows:

$$f_m(k,z)=\frac{1}{\sqrt{\Lambda\Delta}}\times\begin{cases}[\Delta_1+\Delta_5+\Delta_3(e^{2ka}-1)-(\Delta+\Delta_5)e^{-2kb}]e^{kz}\ , & z\le -a\\ [(\Delta_1-\Delta_2)e^{-2ka}+\Delta_3]e^{-kz}+[\Delta_2-\Delta_3+\Delta_5-(\Delta+\Delta_5)e^{-2kb}]e^{kz}\ , & -a\le z\le 0\\ [(\Delta_1-\Delta_2)e^{-2ka}+\Delta_2-\Delta_4+\Delta_5]e^{-kz}+[\Delta_4-(\Delta+\Delta_5)e^{-2kb}]e^{kz}\ , & 0\le z\le b\\ [(\Delta_1-\Delta_2)e^{-2ka}+\Delta_4(e^{2kb}-1)+\Delta_2-\Delta]e^{-kz}\ , & z\ge b\ .\end{cases} \tag{3b}$$

For the definitions of Δ, Δ_1, Δ_2, Δ_3, Δ_4, Δ_5, and Λ, see paper I. By using Eqs. (17) and (23) in paper I and the formula

$$\frac{\eta_\nu}{\omega_{p\nu}^2}=\frac{\epsilon_{\infty\nu}^2(\omega_{L\nu}^2-\omega_{T\nu}^2)^2}{\omega_{T\nu}^2(\epsilon_{0\nu}-\epsilon_{\infty\nu})[\epsilon_{\infty\nu}(\omega_{L\nu}^2-\omega^2)-(\omega_{T\nu}^2-\omega^2)]^2}\ , \tag{4}$$

for the interface modes, we finally obtain the following result:

$$\begin{aligned}\Lambda\Delta^2=&\frac{\Delta_1^2\epsilon_{\infty1}^2(\omega_{L1}^2-\omega_{T1}^2)^2}{\omega_{T1}^2(\epsilon_{01}-\epsilon_{\infty1})\{\epsilon_{\infty1}[\omega_{L1}^2-\omega_m^2(k)]-[\omega_{T1}^2-\omega_m^2(k)]\}^2}e^{-2ka}\\ &+\frac{\epsilon_{\infty2}^2(\omega_{L2}^2-\omega_{T2}^2)^2}{\omega_{T2}^2(\epsilon_{02}-\epsilon_{\infty2})\{\epsilon_{\infty2}[\omega_{L2}^2-\omega_m^2(k)]-[\omega_{T2}^2-\omega_m^2(k)]\}^2}[\Delta_2^2(1-e^{-2ka})-\Delta_3^2(1-e^{2ka})]\\ &+\frac{\epsilon_{\infty3}^2(\omega_{L3}^2-\omega_{T3}^2)^2}{\omega_{T3}^2(\epsilon_{03}-\epsilon_{\infty3})\{\epsilon_{\infty3}[\omega_{L3}^2-\omega_m^2(k)]-[\omega_{T3}^2-\omega_m^2(k)]\}^2}[\Delta_4^2(e^{2kb}-1)-\Delta_5^2(e^{-2kb}-1)]\\ &+\frac{\Delta^2\epsilon_{04}^2(\omega_{L4}^2-\omega_{T4}^2)^2}{\omega_{T4}^2(\epsilon_{04}-\epsilon_{\infty4})\{\epsilon_{\infty4}[\omega_{L4}^2-\omega_m^2(k)]-[\omega_{T4}^2-\omega_m^2(k)]\}^2}e^{-2kb}\ ,\end{aligned} \tag{5}$$

where $\omega_{L\nu}$ and $\omega_{T\nu}$ are the Brillouin-zone-center frequencies of the LO and TO modes, $\nu(=1,2,3,4)$ is the material index, $\epsilon_{0\nu}$ is the static dielectric constant, and $\epsilon_{\infty\nu}$ is the high-frequency dielectric constant.

Let us now briefly discuss the above results in two cases. When $a=b=0$ and $r_2=r_3=0$, from Eqs. (1), (3), and (5) we can obtain the same result as in Table III of Ref. 5 for the single heterostructure model. Moreover, in the case of $a=b$, $r_1=r_4$, and $r_2=r_3$, from Eqs. (1), (3), and (5) we can obtain the same result as in Table IV of Ref. 5 for the double heterostructure (single QW) model. Thus the results obtained in the present study are more general than those in Ref. 5 by Mori and Ando.

B. Electron subbands

Assuming the usual effective-mass approximation for the conduction band, the envelope wave function for the electron in the ith conduction subband in a general step QW (shown in Fig. 1) is obtained from the solution of the Schrödinger equation as follows:

$$\psi_i(z)=B_i\times\begin{cases}\alpha_{1i}\exp(k_{li}z)\ , & z\le -a\\ \alpha_{2i}\sin(k_{wi}z)+\alpha_{3i}\cos(k_{wi}z)\ , & -a\le z\le 0\\ \alpha_{4i}\exp(k_{si}z)+\alpha_{5i}\exp(-k_{si}z)\ , & 0\le z\le b\\ \exp(-k_{ri}z)\ , & z\ge b\ ,\end{cases} \tag{6}$$

where $k_{li}=[2m_l(V_l-E_i)]^{1/2}/\hbar$, $k_{wi}=[2m_wE_i]^{1/2}/\hbar$, $k_{si}=[2m_s(V_s-E_i)]^{1/2}/\hbar$, and $k_{ri}=[2m_r(V_r-E_i)]^{1/2}/\hbar$, with E_i being the ith electron energy level. The electron effective masses (potentials) in the four regions are $m_l(V_l)$, $m_w(0)$, $m_s(V_s)$, and $m_r(V_r)$, respectively, and $\alpha_{ni}(n=1,2,3,4,5)$ in Eq. (6) are defined as follows:

$$\begin{aligned}
&\alpha_{1i}\equiv\gamma_{lwi}\alpha_{3i}\exp(k_{li}a)/[\gamma_{lwi}\cos(k_{wi}a)+\sin(k_{wi}a)]\ ,\\
&\alpha_{2i}\equiv\alpha_{3i}[\cos(k_{wi}a)-\gamma_{lwi}\sin(k_{wi}a)]/[\gamma_{lwi}\cos(k_{wi}a)+\sin(k_{wi}a)]\ ,\\
&\alpha_{3i}\equiv[\cosh(k_{si}b)+\gamma_{sri}\sinh(k_{si}b)]\exp(-k_{ri}b)\ ,\\
&\alpha_{4i}\equiv(1-\gamma_{sri})\exp[-(k_{si}+k_{ri})b]/2\ ,\\
&\alpha_{5i}\equiv(1+\gamma_{sri})\exp[(k_{si}-k_{ri})b]/2\ ,
\end{aligned} \tag{7}$$

where $\gamma_{lwi}=k_{wi}m_l/k_{li}m_w$ and $\gamma_{sri}=k_{ri}m_s/k_{si}m_r$. The subband energy equation in a general step QW is obtained as follows:

$$\begin{aligned}[\cos(k_{wi}a)-\gamma_{lwi}\sin(k_{wi}a)][\cosh(k_{si}b)+\gamma_{sri}\sinh(k_{si}b)]\\ +\gamma_{wsi}[\sinh(k_{si}b)+\gamma_{sri}\cosh(k_{si}b)][\gamma_{lwi}\cos(k_{wi}a)+\sin(k_{wi}a)]=0\ ,\end{aligned} \tag{8}$$

where $\gamma_{wsi}=k_{si}m_w/k_{wi}m_s$.

The constant B_i in Eq. (6) can be determined by the normalization condition as follows:

$$B_i=1/(D_{1i}+D_{2i})^{1/2}\ , \tag{9}$$

where

$$\begin{aligned}D_{1i}=&|\alpha_{1i}|^2\exp(-2k_{li}a)/2k_{li}+a(|\alpha_{2i}|^2+|\alpha_{3i}|^2)/2+(|\alpha_{3i}|^2-|\alpha_{2i}|^2)\sin(2k_{wi}a)/4k_{wi}\\ &+[\cos(2k_{wi}a)-1]\,\mathrm{Re}(\alpha_{2i}^*\alpha_{3i})/2k_{wi}+\exp(-2k_{ri}b)/2k_{ri}\end{aligned} \tag{10a}$$

and

$$D_{2i}=\begin{cases}(|\alpha_{5i}|^2-|\alpha_{4i}|^2)/2k_{si}+[|\alpha_{4i}|^2\exp(2k_{si}b)-|\alpha_{5i}|^2\exp(-2k_{si}b)]/2k_{si}+2b\ \mathrm{Re}(\alpha_{4i}^*\alpha_{5i})\ , & \text{for } k_{si} \text{ real}\ ,\\ (|\alpha_{4i}|^2+|\alpha_{5i}|^2)b+\mathrm{Re}(\alpha_{4i}^*\alpha_{5i})\sin(2|k_{si}|b)/|k_{si}|-\mathrm{Im}(\alpha_{4i}^*\alpha_{5i})[\cos(2|k_{si}|b)-1]/|k_{si}| & \text{for } k_{si} \text{ imaginary}\ .\end{cases} \tag{10b}$$

Here Re and Im denote real and imaginary parts, respectively.

C. Electron–interface-phonon scattering

In this subsection, as an application of the interaction Hamiltonian given in Sec. II A we consider a one-phonon process. The electron–interface-phonon-scattering rates in a four-layer heterostructure can be obtained from the usual Fermi golden rule

$$\begin{aligned}W^{(i\to f)}(k_i)&=\frac{2\pi}{\hbar}\int dN_f\,\delta[\varepsilon_i-\varepsilon_f\pm\hbar\omega(k)]|\langle\mathbf{k}_f|H_{e-\mathrm{ph}}|\mathbf{k}_k\rangle|^2\\ &=\frac{e^2}{16\pi\varepsilon_0}\sum_m\int d^2\mathbf{k}\frac{1}{\omega_m(k)k}|F_m(k)|^2\delta[\varepsilon_i-\varepsilon_f\pm\hbar\omega_m(k)](N_{\mathrm{ph}}+\tfrac{1}{2}\mp\tfrac{1}{2})\delta_{\mathbf{k}_i,\mathbf{k}_f\mp\mathbf{k}}\ ,\end{aligned} \tag{11}$$

where N_{ph} is the interface-phonon occupation number, the upper sign is for phonon absorption, and the lower is for emission. $F_m(k)$ is the overlap integration defined as

$$F_m(k)=\int_{-\infty}^{\infty}\psi_f^*(z)f_m(k,z)\psi_i(z)dz\ , \tag{12}$$

where $f_m(k,z)$ is given in Eq. (3b) and ψ_i and ψ_f are the electron envelope subband wave functions in the initial and final states, respectively. The total electron energy ε is written as the sum of parallel and transverse components:

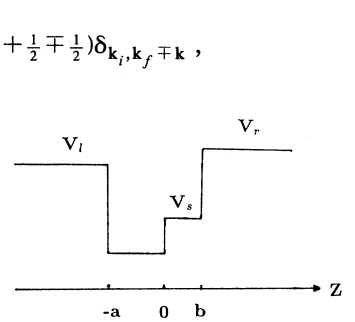

FIG. 1. Geometry of a general step QW structure. Here V_s, V_l, and V_r respectively, denote the step height, the left barrier height, and the right barrier height; a is the well width; and b the step width.

$$\varepsilon=\frac{\hbar^2 k_e^2}{2m^*}+E \ , \tag{13}$$

where $\mathbf{k}_e$ is the electron wave vector in the xy plane parallel to the interface. E can be obtained by solving the subband energy equation (8).

For intrasubband scattering within the first subband, we consider the scattering rate $W^{(1\to1)}$ for phonon emission. Assuming that the electron energy is just enough to emit one interface phonon, from Eq. (11) we can obtain

$$W^{(1\to1)}=\frac{e^2}{8\varepsilon_0}\sum_m \frac{1}{\omega_m(k_{11})}|F_m(k_{11})|^2 \times\left[\left|\frac{\hbar^2}{m^*}k_{11}-\hbar\frac{d\omega_m}{dk}\bigg|_{k_{11}}\right|\right]^{-1} \times(N_{\rm ph}+1) \ , \tag{14}$$

where k_{11} satisfies

$$\frac{\hbar^2}{2m^*}k_{11}^2-\hbar\omega_m(k_{11})=0 \ . \tag{15}$$

For the intersubband transition between the first and second subbands, we still consider the scattering rate $W^{(2\to1)}$ for phonon emission. Assuming that the electron is initially at the bottom of the second subband, we have

$$W^{(2\to1)}=\frac{e^2}{8\varepsilon_0}\sum_m \frac{1}{\omega_m(k_{21})}|F_m(k_{21})|^2 \times\left[\left|\frac{\hbar^2}{m^*}k_{21}+\hbar\frac{d\omega_m}{dk}\bigg|_{k_{21}}\right|\right]^{-1} \times(N_{\rm ph}+1) \ , \tag{16}$$

where k_{21} satisfies

$$\frac{\hbar^2 k_{21}^2}{2m^*}+\hbar\omega_m(k_{21})-(E_2-E_1)=0 \ , \tag{17}$$

and (E_2-E_1) is the energy difference between the first and second subbands.

III. NUMERICAL RESULTS AND DISCUSSION

In order to see more clearly the behaviors of the electron–interface-phonon interaction and scattering in asymmetric QW structures, we have calculated the coupling function $\Gamma(k,z)$ and scattering rates in GaAs/Al_xGa_{1-x}As QW structures. The parameters used in our calculations are as follows. The potential height of $Al_xGa_{1-x}As$ is determined by $V(x)=0.6(1266x+260x^2)$ meV.[16] The corresponding electron effective mass is given by $m_e=(0.0665+0.0835x)m_0$,[17] where m_0 is the free-electron mass. The dielectric constants $\epsilon_0=13.18-3.12x$ and $\epsilon_\infty=10.89-2.73x$.[18] The bulk phonon energies[18] $\hbar\omega_{\rm LO}(x)=36.25-6.55x+1.79x^2$ meV and $\hbar\omega_{\rm TO}(x)=33.29-0.64x-1.16x^2$ meV (GaAs type). For an investigation of the $|\Gamma(k,z)|-k$ relation in symmetric and asymmetric single QW's, commonly used step QW's, and general step QW's, we have chosen four typical examples with structure parameters shown in Table I.

Figure 2 shows the $\Gamma(k,z)-z$ relation for sample 4, where (a) is for the three lower-frequency modes 1, 2, and 3, and (b) is for the three higher-frequency modes 4, 5, and 6. The plots indicate that the electron interaction with modes 2 and 5]denoted as e-$p(2)$ and e-$p(5)$, respectively] are mainly localized in the vicinity of the left interface (at $z=-100$ Å); the e-$p(3)$ and e-$p(6)$ peaks at the middle interface ($z=0$); and the e-$p(1)$ and e-$p(4)$ peaks at the right interface ($z=50$ Å). Moreover, from Fig. 2 and numerical results for other layered structures, we can conclude that the higher-frequency modes are much more important for the electron-phonon interaction than the lower-frequency modes. Paper I indicates that, in the long-wavelength limit, the frequency magnitudes of all the higher-frequency modes are greater than or equal to $\omega_{\rm LO}(0)$ and those of all the lower-frequency modes are greater than or equal to $\omega_{\rm TO}(0)$ and less than $\omega_{\rm LO}(0)$. For simplicity, we denote hereafter the higher-frequency modes as interface LO modes, and the lower-frequency modes as interface TO modes.

Figure 3 shows the absolute values $|\Gamma(k,z)|$ as functions of k for samples 1 and 2 in Figs. 3(a) and 3(b), respectively. We can see that the behavior of the $|\Gamma(k,z)|-k$ relation for interface modes 2, 3, and 4 in the symmetric single QW is analogous to that in the asymmetric one. However, the behavior of the $|\Gamma(k,z)|-k$ relation for the first interface mode has an obvious difference in the symmetric and asymmetric QW's. In comparison with the negligibly small interaction between the electron and the first interface mode in the symmetric single QW, as shown in Fig. 3(a), the e-$p(1)$ interaction is quite large in the vicinity of the Brillouin-zone center in the asymmetric single QW as shown in Fig. 3(b). This anomalous behavior can be related to the previously mentioned (in paper I) frequency-forbidden phenomenon in asymmetric layered structures. In a symmetric single QW, the long-wavelength limit of the first interface mode

TABLE I. Sample parameters.

Sample number	Structure	Well width (Å)	Step width (Å)
1	$Al_{0.35}Ga_{0.65}As/GaAs/Al_{0.35}Ga_{0.65}As$	100	0
2	$Al_{0.35}Ga_{0.65}As/GaAs/Al_{0.4}Ga_{0.6}As$	100	0
3	$Al_{0.35}Ga_{0.65}As/GaAs/Al_{0.2}Ga_{0.8}As/Al_{0.35}Ga_{0.65}As$	100	50
4	$Al_{0.35}Ga_{0.65}As/GaAs/Al_{0.2}Ga_{0.8}As/Al_{0.4}Ga_{0.6}As$	100	50

is equal to the bulk TO mode of the side (barrier) material. It is well known that the electron does not couple to TO-phonon modes of p polarization because the TO modes are not accompanied by the appearance of surface or bulk polarization charges.[15] Hence the e-$p(1)$ interaction is extremely small in a symmetric single QW, and this behavior has been quantitatively shown in Fig. 3(a).[19] In an asymmetric single QW (e.g., sample 2), on the other hand, the long-wavelength limit of the first interface mode is a frequency ω_- [see Eqs. (30b) and (32) of paper I] which is not the TO frequency of the barrier material ($Al_{0.35}Ga_{0.65}As$ or $Al_{0.4}Ga_{0.6}As$ in our sample) (and thus called the forbidden frequency of the side materials). The interface mode with the long-wavelength frequency ω_- may cause a polarization in media and hence the e-$p(1)$ interaction in an asymmetric single QW can be much stronger than that in a symmetric single QW, as shown in Fig. 3. Incidentally, it is well known that the dispersion relation for the interface modes in a single heterostructure is $\epsilon_1(\omega)+\epsilon_2(\omega)=0$ [see Eq. (2.10) of Ref. 5], its solutions are $\omega_\pm$ which are similar to Eq. (30b) of paper I. Moreover, the results of Table III in Ref. 5 clearly show that the interaction between an electron and the interface

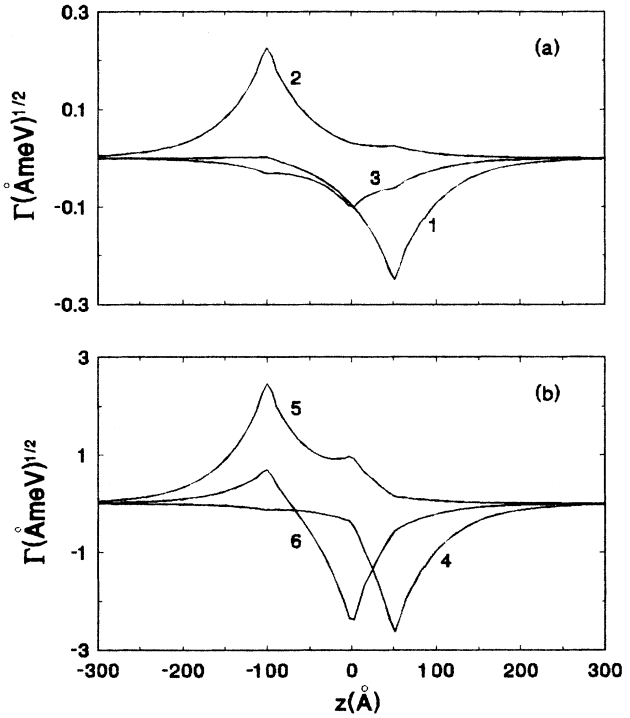

FIG. 2. Spatial dependence of the electron–interface-phonon coupling function $\Gamma(k,z)$ divided by $(\hbar e^2/A\varepsilon_0)^{1/2}$ for a general step QW $Al_{0.35}Ga_{0.65}As/GaAs/Al_{0.2}Ga_{0.8}As/Al_{0.4}Ga_{0.6}As$ (GaAs type) with 100-Å GaAs and 50 Å $Al_{0.2}Ga_{0.8}As$, and $k=0.02$ Å^{-1}. Here and in Figs. 3–8, the numbers by the curves represent the interface phonon frequency in order of increasing magnitude (a) for the three lower-frequency modes; and (b) for the three higher-frequency modes.

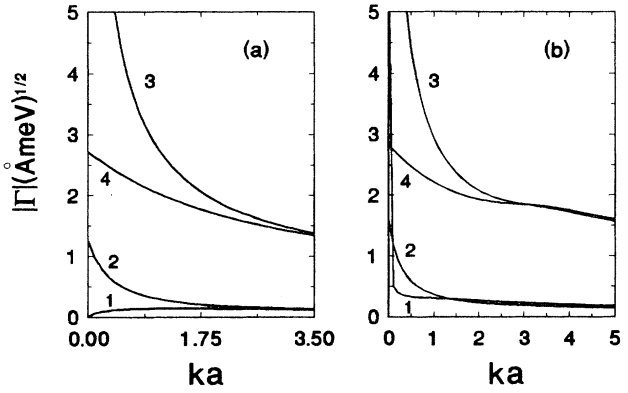

FIG. 3. Absolute values $|\Gamma(k,z)|$ divided by $(\hbar e^2/A\varepsilon_0)^{1/2}$ as functions of k, (a) for an $Al_{0.35}Ga_{0.65}As/GaAs/Al_{0.35}Ga_{0.65}As$ symmetric QW and (b) for an $Al_{0.35}Ga_{0.65}As/GaAs/Al_{0.4}Ga_{0.6}As$ asymmetric single QW. Here well width $a=100$ Å for both QW's.

modes with frequencies $\omega_\pm$ is important. Thus the frequency-forbidden behavior and its significant influence to the electron–interface-phonon interaction may be a common phenomenon for asymmetric heterostructures.

The $|\Gamma(k,z)|$-k relation for samples 3 and 4 are shown in Figs. 4(a) and 4(b), respectively. We can see that the interaction between an electron and interface modes 2, 3, 4, 5, and 6 in the commonly used step QW is analogous to that of the general step QW. However, in the vicinity of the Brillouin-zone center, the e-$p(1)$ interaction of the general step QW (sample 4) is much stronger than that in the commonly used step QW (sample 3). The physical origin of this anomaly is similar to that for the asymmetric single QW mentioned above. That is, since the long-wavelength limit of the first interface mode is a frequency ω_- different from the TO frequencies of the side materials ($Al_{0.35}Ga_{0.65}As$ and $Al_{0.4}Ga_{0.6}As$), it can produce a polarization and a large interaction with the electron.

Figures 4(a) and 4(b) also show that the interaction between an electron and the fifth interface mode has a maximum at $k(a+b)\doteq 0.9$. In order to clarify the physical origin of this anomalous behavior in the $|\Gamma(k,z)|$-k relation, we have carefully analyzed the corresponding dispersion plots (ω_5-k) for the fifth interface mode (these plots are similar to the fifth branch of Fig. 3 in paper I) and have found that the ω_5-k plots for the two step QW's have an inflection point located at $k(a+b)\doteq 0.9$. That is, the maximal point of the $|\Gamma(k,z)|$-k plots exactly corresponds to the inflection point in the dispersion relation. We have also noted that the inflection does not exist in the dispersion (ω_j-k) plots for the interface modes other than the fifth mode (i.e., $j\neq 5$). Thus we can conclude that the inflection of the dispersion relation significantly strengthens the electron–interface-phonon interaction. The appearance of the inflection in the ω_5-k relation and its intimate relation to the polarization effect can be explained as follows. The $\Gamma(k,z)-z$ plots in Figs. 2(a) and 2(b) suggest that the polarization effect of interface

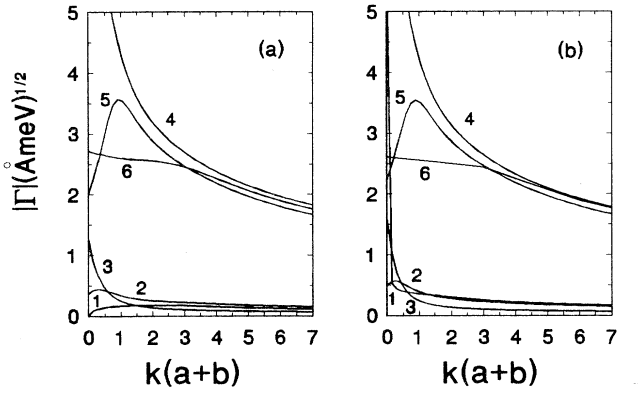

FIG. 4. Same as in Fig. 3, but (a) for a commonly used step QW $Al_{0.35}Ga_{0.65}As/GaAs/Al_{0.2}Ga_{0.8}As/Al_{0.35}Ga_{0.65}As$ and (b) for a general step QW $Al_{0.35}Ga_{0.65}As/GaAs/Al_{0.2}Ga_{0.8}As/Al_{0.4}Ga_{0.6}As$. Here well width $a=100$ Å and step width $b=50$ Å for both QW's.

LO modes 4, 5, and 6 is much stronger than that of the interface TO modes 1, 2 and 3. Notable mutual polarization effects may exist among the interface LO modes. In particular, mode 6 can possibly give the strongest and most complex influence to mode 5 [see Fig. 2(b)], while the effect of mode 6 on mode 4 may be weaker. Moreover, Fig. 2(b) also suggests that the effect of mode 4 on mode 5 is negligible, and the effects of modes 4 and 5 on mode 6 may be opposite in sign and so partly cancel each other. Thus it is understandable that the inflection behavior only appears on the dispersion relation for the fifth mode.

In the above we have pointed out that the values of the electron-phonon coupling strength $|\Gamma(k,z)|$ for interface LO modes are larger than those for interface TO modes. Our calculation of electron–interface-phonon-scattering rates has also shown that the interface LO modes are much more important than the interface TO modes. Hence we ignore the electron–interface-TO-phonon-scattering rates in the following calculations.

In Fig. 5 we show the scattering rates divided by $(N_{\text{ph}}+1)$ as functions of well width for intrasubband $(1\rightarrow 1)$ and intersubband $(2\rightarrow 1)$ electronic transitions due to interface LO phonons in $Al_{0.35}Ga_{0.65}As/GaAs/Al_{0.4}Ga_{0.6}As$ asymmetric single QW's, where solid curves 1 and 2 represent the contribution of individual interface LO modes in the order of increasing magnitude of frequency, and the solid curve W_t represents the total scattering rate. For comparison, the dashed curves show our calculation results for $Al_{0.36}Ga_{0.64}As/GaAs/Al_{0.36}Ga_{0.64}As$ symmetric single QW's. These results are in agreement with those of Figs. 5 and 6 in Ref. 10. Moreover, we know that in a strictly symmetric QW the intrasubband $(1\rightarrow 1)$ transition involves only symmetric phonons (mode 1), and that the contribution from the antisymmetric mode 2 is zero, while the intersubband $(2\rightarrow 1)$ transition involves only antisymmetric phonons (mode 2) and the contribution from the symmetric mode

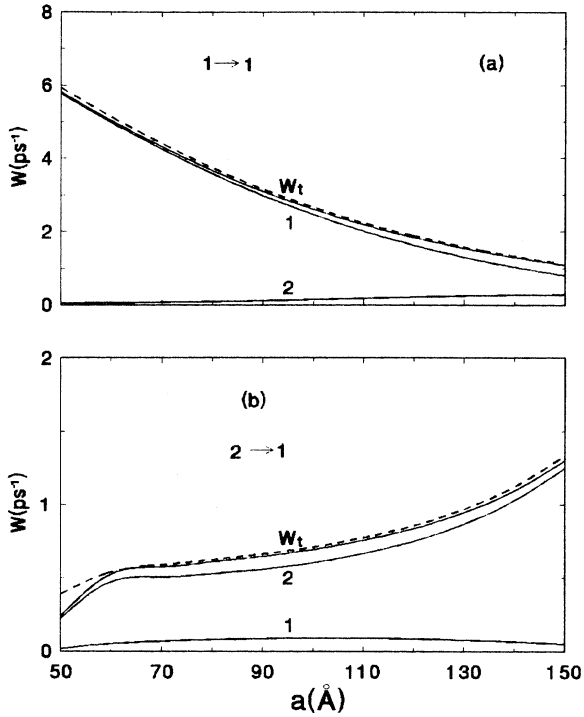

FIG. 5. Intrasubband (a) and intersubband (b) scattering rates as functions of well width a for $Al_{0.35}Ga_{0.65}As/GaAs/Al_{0.4}Ga_{0.6}As$ asymmetric single QW's for each interface LO mode and their summation W_t. The dashed curve represents the scattering rate for $Al_{0.36}Ga_{0.64}As/GaAs/Al_{0.36}Ga_{0.64}As$ symmetric single QW's.

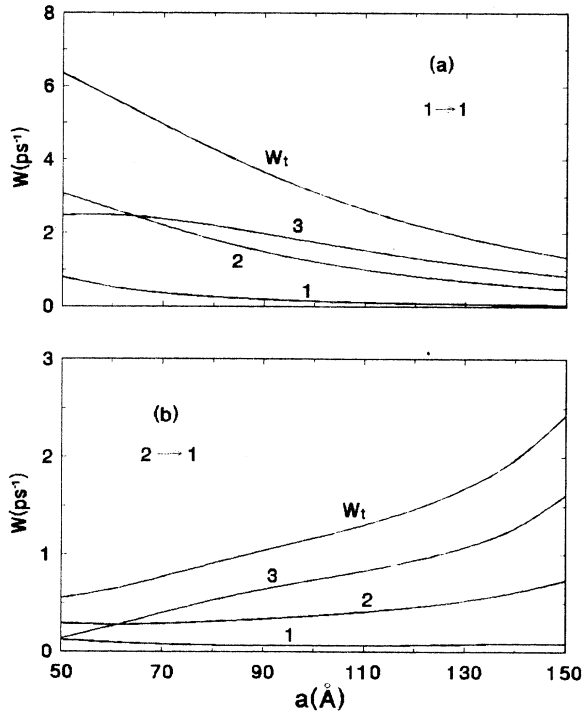

FIG. 6. Intrasubband (a) and intersubband (b) scattering rates as functions of well width a for $Al_{0.35}Ga_{0.65}As/GaAs/Al_{0.1}Ga_{0.9}As/Al_{0.4}Ga_{0.6}As$ step QW's with step width $b=50$ Å.

1 is zero. These usual selection rules will break down if the QW potential has any asymmetry,[14] since in this case phonon mode 1 and the first subband electronic state $\psi_1(z)$ are not strictly symmetric, and mode 2 and the second subband state $\psi_2(z)$ are not strictly antisymmetric. Thus the intrasubband $(1\rightarrow 1)$ scattering for phonon mode 2 and the intersubband $(2\rightarrow 1)$ scattering for mode 1 are not completely forbidden. However, if the asymmetry of the QW potential is not serious, mode 1 (2) can still dominate in the $(1\rightarrow 1)$ intrasubband [$(2\rightarrow 1)$ intersubband] transition. For example, if we measure the asymmetry degree of the QW $Al_{0.35}Ga_{0.65}As/GaAs/Al_{0.4}Ga_{0.6}As$ to be approximately $|V_r - V_l|/V_r \approx 0.1$, we can estimate that the contribution of mode 2 (1) to the $(1\rightarrow 1)$ intrasubband [$(2\rightarrow 1)$ intersubband] scattering should be one order of magnitude smaller than that of the dominant mode 1 (2). This rough estimate is in semiquantitative agreement with the corresponding exactly calculated results shown in Figs. 5(a) and 5(b).

Figure 5(b) also shows that the total intersubband scattering rate for the asymmetric QW's (solid curve W_t) deviates from that for the symmetric QW's (dashed curve) even at large well widths. This is mainly due to the fact that asymmetric and symmetric QW's (with the same well width) have different values of the overlap integration [Eq. (12)].

Figure 6 shows the scattering rates as functions of well width a for $Al_{0.35}Ga_{0.65}As/GaAs/Al_{0.1}Ga_{0.9}As/Al_{0.4}Ga_{0.6}As$ step QW's, where the step width b is fixed at 50 Å. We can see again that the usual selection rules break down in these asymmetric heterostructures. Moreover, in the case when the second subband energy level crosses the step height, i.e., $E_2(\approx V_s)\approx 77.52$ meV (corresponding to $a\approx 120$ Å), the scattering rates have no obvious changes. From Eqs. (6), (7), (9), (10), (12), and (17) we can see that k_{21} and $F_m(k_{21})$ are continuous functions of E_1 and E_2, hence the scattering rates $W^{(2\rightarrow 1)}$ have no obvious changes in the case that E_2 crosses the step height.

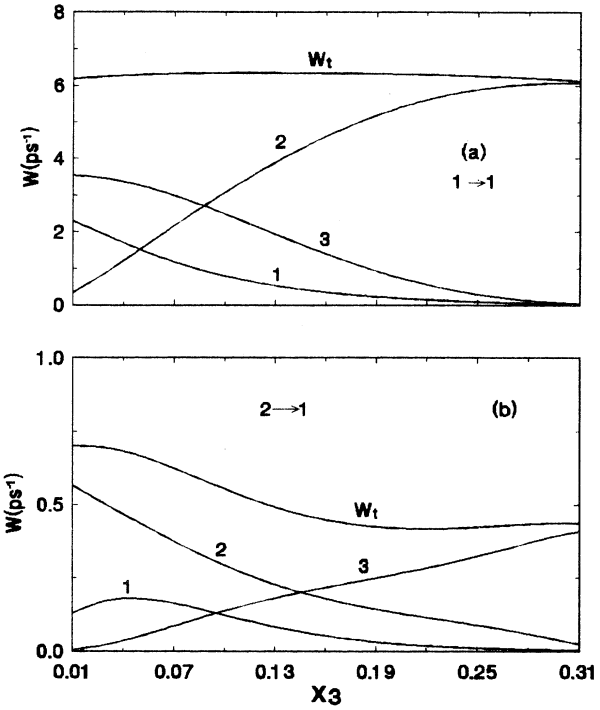

FIG. 8. Intrasubband (a) and intersubband (b) scattering rates as functions of x_3 for $Al_{0.35}Ga_{0.65}As/GaAs/Al_{x_3}Ga_{1-x_3}As/Al_{0.4}Ga_{0.6}As$ step QW's with well width $a=50$ Å and step width $b=50$ Å.

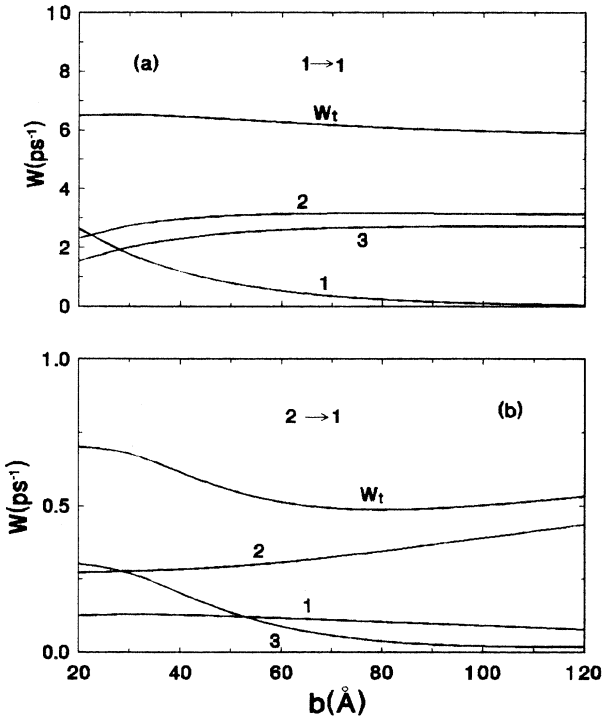

FIG. 7. Intrasubband (a) and intersubband (b) scattering rates as functions of step width b for $Al_{0.35}Ga_{0.65}As/GaAs/Al_{0.1}Ga_{0.9}As/Al_{0.4}Ga_{0.6}As$ step QW's with well width $a=50$ Å.

Figure 7 shows the scattering rates as functions of step width b for $Al_{0.35}Ga_{0.65}As/GaAs/Al_{0.1}Ga_{0.9}As/Al_{0.4}Ga_{0.6}As$ step QW's, where the well width a is fixed at 50 Å. Figure 7(a) indicates that the intrasubband scattering rate W_t is an insensitive function of step width, while Fig. 7(b) shows that the intersubband scattering rate W_t is a complicated function of b.

Figure 8 shows the scattering rates as a function of the Al mole fraction x_3 for $Al_{0.35}Ga_{0.65}As/GaAs/Al_{x_3}Ga_{1-x_3}As/Al_{0.4}Ga_{0.6}As$ step QW's, where well width $a=50$ Å and step width $b=50$ Å. We can see that the intrasubband scattering rate W_t is an insensitive function of x_3, while the intersubband scattering rate W_t is a complicated function of x_3.

We have also calculated the scattering rates for commonly used step QW's. The situations are similar to those of general step QW's shown in Figs. 6–8.

IV. SUMMARY

In this paper the interaction Fröhlich-like Hamiltonian between an electron and interface optical phonons and the electron–interface-phonon-scattering rates in asymmetric single and step QW structures have been given. The main results obtained in the present paper are as follows.

(1) The interface LO modes are in general more important than the interface TO modes for the electron-phonon interaction and scattering in heterostructures.

(2) The electron–interface-phonon coupling strength as a function of wave number k has two anomalies. One is that, in asymmetric single QW's and general step QW's, the electron interaction with the lowest frequency interface mode is large in the vicinity of the Brillouin-zone center, and this anomaly indicates that the forbidden frequency mode (see paper I) may cause an obvious polarization and interaction with an electron. The second anomaly is that in step QW's the electron interaction with the fifth interface mode has a maximum relating to the inflection point of the ω_5-k relation, and this fact suggests that the existence of the inflection in the dispersion relation significantly strengthens the corresponding electron-phonon interaction.

(3) The electron scattering depends strongly on the potential parameters, and the usual selection rules for the intrasubband and intersubband transitions break down in asymmetric QW structures, in accordance with the opinion of Jain and Sarma.[14]

(4) In a step QW structure, the total intrasubband scattering rate is an insensitive function of step height and step width, while the intersubband scattering rate is a complicated function of step height and step width.

(5) The scattering rates are continuous functions of the electron subband energy E. In particular, they have no obvious changes when E crosses the step height.

We expect that the results obtained in this paper may motivate further experimental and theoretical studies of the electron-phonon interaction and carrier relaxation mechanism in asymmetric QW structures such as asymmetric single and step QW's, which are of great practical importance.

ACKNOWLEDGMENTS

One of the authors (J.S.) would like to thank Professor Z. X. Liu for helpful discussions. This work was supported by the Natural Science Foundation of China (69406004) and the Natural Science Foundation of Henan Province in China (934060500).

---

*Mailing address.

[1]D. L. Lin, R. Chen, and T. F. George, Solid State Commun. **73**, 799 (1990); R. Chen, D. L. Lin, and T. F. George, Phys. Rev. B **41**, 1435 (1990).

[2]D. L. Lin, R. Chen, and T. F. George, Phys. Rev. B **43**, 9328 (1991).

[3]D. L. Lin, R. Chen, and T. F.George, J. Phys. Condens. Matter **3**, 4645 (1991).

[4]Xi-xia Liang and Xu Wang, Phys. Rev. B **43**, 5155 (1991).

[5]N. Mori and T. Ando, Phys. Rev. B **40**, 6175 (1989).

[6]R. Lassnig, Phys. Rev. B **30**, 7132 (1984); E. P. Pokatilov, V. M. Fomin, N. N. Semenovskaya, and S. I. Beril, *ibid.* **47**, 16 597 (1993).

[7]Xi-xia Liang, J. Phys. C **4**, 9769 (1992); X. X. Liang and S. G. Davison, Solid State Commun. **84**, 581 (1992); Surf. Sci. **298**, 225 (1993).

[8]Jun-jie Shi and Shao-hua Pan, Phys. Rev. B **46**, 4265 (1992).

[9]Jun-jie Shi, Ling-xi Shangguan, and Shao-hua Pan, Phys. Rev. B **47**, 13 471 (1993).

[10]Wenhui Duan, Jia-Lin Zhu, and Bing-Lin Gu, J. Phys. Condens. Matter **5**, 2859 (1993).

[11]G. Weber, J. Phys. C **4**, 9831 (1992); Solid State Commun. **84**, 595 (1992).

[12]K. W. Kim, A. R. Bhatt, M. A. Stroscio, P. J. Turley, and S.W. Teitsworth, J. Appl. Phys. **72**, 2282 (1992).

[13]Wenhui Duan, Jia-Lin Zhu, and Bing-Lin Gu, Phys. Rev. B **49**, 14 403 (1994).

[14]J. K. Jain and S. D. Sarma, Phys. Rev. Lett. **62**, 2305 (1989).

[15]L.Wendler, Phys. Status Solidi B **129**, 513 (1985).

[16]M. A. A. Afromowitz, Solid State Commun. **15**, 59 (1974); D. F. Nelson, R. C. Miller, and D. A. Kleinman, Phys. Rev. B **35**, 7770 (1987).

[17]D. A. B. Miller, D. S. Chemla, T. C. Damen, A. C. Gossard, W. Wiegmann, T. H. Wood, and C. A. Burrus, Phys. Rev. Lett. **53**, 2173 (1984).

[18]S. Adachi, J. Appl. Phys. **58**, R1 (1985).

[19]Compared with the previously calculated result of Ref. 4, we can see that our result in Fig. 3(a) is inconsistent with that of Liang and Wang (Ref. 4). From Eqs. (17) and (26) of Ref. 4 we can also conclude that the numerical result of that reference has an error in the limiting case of $k \rightarrow 0$. In the case of a symmetric single QW, the known result of Mori and Ando (Ref. 5) can be reproduced from our results (see Sec. II A). Moreover, for sample 1 we have calculated the coupling function by using the analytical expression of Ref. 5; the result is the same as ours given in Fig. 3(a). Hence we believe that the numerical result in Fig. 3(a) should be reliable.